Galaxy And Mass Assembly (GAMA): stellar mass growth of spiral galaxies in the cosmic web

Article (Published Version)

Monthly Notices
of the
ROYAL ASTRONOMICAL SOCIETY
MNRAS **457,** 2287–2300 (2016) doi:10.1093/mnras/stw134

Galaxy And Mass Assembly (GAMA): stellar mass growth of spiral galaxies in the cosmic web

Mehmet Alpaslan,[1⋆] Meiert Grootes,[2] Pamela M. Marcum,[1] Cristina Popescu,[2,3,4] Richard Tuffs,[2] Joss Bland-Hawthorn,[5] Sarah Brough,[6] Michael J. I. Brown,[7] Luke J. M. Davies,[8] Simon P. Driver,[8] Benne W. Holwerda,[9] Lee S. Kelvin,[10] Maritza A. Lara-López,[11] Ángel R. López-Sánchez,[6,12] Jon Loveday,[13] Amanda Moffett,[8] Edward N. Taylor,[14] Matt Owers[6,12] and Aaron S. G. Robotham[8]

[1]*NASA Ames Research Center, N232, Moffett Field, Mountain View, CA 94035, USA*
[2]*Max Planck Institute fuer Kernphysik, Saupfercheckweg 1, D-69117 Heidelberg, Germany*
[3]*Jeremiah Horrocks Institute, University of Central Lancashire, PR1 2HE Preston, UK*
[4]*The Astronomical Institute of the Romanian Academy, Str. Cutitul de Argint 5, 040557 Bucharest, Romania*
[5]*Sydney Institute for Astronomy, School of Physics A28, University of Sydney, NSW 2006, Australia*
[6]*Australian Astronomical Observatory, PO Box 915, North Ryde, NSW 1670, Australia*
[7]*School of Physics and Astronomy, Monash University, Clayton, VIC 3800, Australia*
[8]*International Centre for Radio Astronomy Research, 7 Fairway, The University of Western Australia, Crawley, Perth, WA 6009, Australia*
[9]*University of Leiden, Sterrenwacht Leiden, Niels Bohrweg 2, NL-2333 CA Leiden, the Netherlands*
[10]*Astrophysics Research Institute, Liverpool John Moores University, IC2, Liverpool Science Park, 146 Brownlow Hill, Liverpool L3 5RF, UK*
[11]*Instituto de Astronomía, Universidad Nacional Autónoma de México, A.P. 70-264, 04510 México, D.F., México*
[12]*Department of Physics and Astronomy, Macquarie University, NSW 2109, Australia*
[13]*Astronomy Centre, University of Sussex, Falmer, Brighton BN1 9QH, UK*
[14]*School of Physics, The University of Melbourne, Parkville, VIC 3010, Australia*

Accepted 2016 January 13. Received 2015 December 22; in original form 2015 October 20

ABSTRACT

We look for correlated changes in stellar mass and star formation rate (SFR) along filaments in the cosmic web by examining the stellar masses and UV-derived SFRs of 1799 ungrouped and unpaired spiral galaxies that reside in filaments. We devise multiple distance metrics to characterize the complex geometry of filaments, and find that galaxies closer to the cylindrical centre of a filament have higher stellar masses than their counterparts near the periphery of filaments, on the edges of voids. In addition, these peripheral spiral galaxies have higher SFRs at a given mass. Complementing our sample of filament spiral galaxies with spiral galaxies in tendrils and voids, we find that the average SFR of these objects in different large-scale environments are similar to each other with the primary discriminant in SFR being stellar mass, in line with previous works. However, the distributions of SFRs are found to vary with large-scale environment. Our results thus suggest a model in which in addition to stellar mass as the primary discriminant, the large-scale environment is imprinted in the SFR as a second-order effect. Furthermore, our detailed results for filament galaxies suggest a model in which gas accretion from voids on to filaments is primarily in an orthogonal direction. Overall, we find our results to be in line with theoretical expectations of the thermodynamic properties of the intergalactic medium in different large-scale environments.

Key words: galaxies: spiral – galaxies: stellar content – large-scale structure of Universe.

1 INTRODUCTION

When viewed at large scales, the distribution of galaxies in the Universe forms a vast network of interconnected filamentary structures, sheets and clusters; all of which surround mostly empty voids. Commonly referred to as the cosmic web or the large-scale structure of

⋆ E-mail: mehmet.alpaslan@nasa.gov

the Universe, this arrangement of galaxies is a direct consequence of perturbations in the initial density field of matter shortly after the big bang evolving under the influence of gravity over cosmic time (Zel'dovich 1970; Shandarin & Zeldovich 1989; Bond, Kofman & Pogosyan 1996). A number of sophisticated algorithms now exist to identify and characterize large-scale structure in observed and simulated data sets (e.g. El-Ad & Piran 1997; Doroshkevich et al. 2004; Aragón-Calvo et al. 2007; Colberg 2007; Hahn et al. 2007; Platen, Van De Weygaert & Jones 2007; Neyrinck 2008; Forero-Romero et al. 2009; Aragón-Calvo, van de Weygaert & Jones 2010; Sousbie 2011; Cautun, van de Weygaert & Jones 2012; Alpaslan et al. 2014a; Tempel et al. 2014; Eardley et al. 2015).

Many mechanisms that drive the evolution of a galaxy are sensitive to the environment in which it resides; particularly the local dark matter (DM) distribution (e.g. Brown et al. 2008; Yang, Mo & van den Bosch 2009; Zheng et al. 2009; Zehavi et al. 2011). One must therefore take environment into account when studying the properties of galaxies; both locally (i.e. the properties of the group or pair in which the galaxy may reside) and globally (whether or not the galaxy resides in a filament or void). The relationship between a galaxy and its local environment is well studied, particularly in the context of its stellar population. Galaxies in groups and pairs often have star formation rates (SFR) that deviate from those found in similar galaxies in the field (e.g. Robotham et al. 2013; Davies et al. 2015). The degree to which large-scale structure impacts galaxy evolution is, however, less thoroughly studied. Recent work has shown that galaxies in voids have somewhat higher specific star formation rates (SSFRs) compared to their counterparts in more dense environments (e.g. Rojas et al. 2004, 2005; Kreckel, Ryan Joung & Cen 2011; Kreckel et al. 2012; Ricciardelli et al. 2014); though Penny et al. (2015) find that void galaxies with stellar masses $>5 \times 10^9$ $M_\odot$ have largely ceased to form stars. Penny et al. (2015) also find that the colour–mass relationship of galaxies does not differ greatly between galaxies in voids and other environments. Concurrently, Fadda et al. (2008) and Darvish et al. (2014) find that there is an enhancement in the fraction of star-forming galaxies in filaments near large clusters.

Beyond the local Universe, there are strong indications that filaments served as conduits for galaxies to accumulate chemically evolved gas at $z \sim 3$; gas which is subsequently converted to young stars (Kereš et al. 2005; Gray & Scannapieco 2013) through enhanced SFRs. A recent study by Snedden et al. (2016) indeed shows that in a suite of simulated filaments, SFRs of galaxies at $z \sim 3$ close to the centre of a filament are lower compared to those in its periphery. Recently, Cautun et al. (2014) have shown that galaxies that reside in filaments at $z = 2$ remain in filaments or migrate into clusters by $z = 0$; therefore, galaxies that have formed in filaments experience a significant alteration of their masses and dynamics through filamentary flows, and then remain within such environments as they evolve. Such an evolutionary history is significantly different from a galaxy residing in an underdense void. In the local Universe, the effect of large-scale structure on galaxy stellar populations has been observed in the cases of galaxies collapsing into superclusters via filaments (e.g. Brough et al. 2006; Porter et al. 2008; Mahajan, Raychaudhury & Pimbblet 2012).

Recently, Alpaslan et al. (2015) concluded that stellar mass is the predominant factor of galaxy properties in the local Universe, as compared to gross environment (e.g. filament versus void; see fig. 15 in Alpaslan et al. 2015, see also Wijesinghe et al. 2012). This paper asks a complementary question: does the location of a galaxy relative to large-scale filaments, the presumed channels of gas flow over cosmic time, predispose the galaxy to higher or lower stellar mass growth (either in the past or currently ongoing in the form of star formation activity)? Specifically, we investigate what impact a galaxy's placement within a filament has on its stellar population, both integrated over its life (stellar mass) and the younger stellar component (UV-derived SFR), with the assumption that the properties and availability of gas vary with filament position. Our study is conducted exclusively on spiral galaxies free of morphological peculiarities, detected nuclear activity, and which are not a member of a galaxy group or pair.

We describe our data in Section 2, from our large-scale structure catalogue and spiral galaxy selection to our UV-derived SSFRs. Section 3 focuses on our analysis, the results of which are subsequently discussed in Section 4. Section 5 provides a summary and conclusion. Throughout this paper, consistent with the cosmology used in Alpaslan et al. (2014a), we adopt $\Omega_{\rm m} = 0.25, \Omega_\Lambda = 0.75, H_0 = h\,100\,{\rm km\,s^{-1}\,Mpc^{-1}}$.

2 DATA

2.1 GAMA and large-scale structure

The characterization of filaments is considerably challenging, due in large part to the complex morphologies of these structures. Observationally, studies of filaments require galaxy redshift surveys that are both highly complete, and have a high target density. One such survey is the Galaxy And Mass Assembly (GAMA, Driver et al. 2009, 2011; Hopkins et al. 2013; Liske et al. 2015; Driver et al. 2016) survey, which combines spectroscopic data obtained at the Anglo-Australian Telescope (AAT, NSW, Australia) with multiwavelength (*UV-FIR*) photometric data from a number of ground- and space-based facilities. The spectroscopic campaign of the survey provides 250 000 spectra for galaxies across five fields; $\alpha =$ 9 h, $\delta = 0.^\circ5$ (G09), $\alpha = 12$ h, $\delta = -0.^\circ5$ (G12) and $\alpha = 14$ h 30 min, $\delta = 0.^\circ5$ (G15), $\alpha = 2$ h, $\delta = -8.^\circ125$ (G02) and $\alpha = 23$ h and $\delta = -32.^\circ5$ (G23). The three equatorial fields (G09, G12 and G15) are 12×5 degrees each, and the two southern fields (G02 and G23) are respectively 8.6×2.5 and 12×5 degrees. The survey is >98 per cent complete down to $m_r = 19.8$ mag. See Driver et al. (2016) for a detailed description of how all this data are homogenized and assimilated into a cohesive photometry catalogue, and Liske et al. (2015) for details on the spectroscopic component of the survey. The high target density and spectroscopic completeness of GAMA enables this work to be a comprehensive search for correlations between large-scale structure and galaxy evolution.

A volume limited galaxy catalogue of 11 791 objects was constructed as a subset of the GAMA Large-Scale Structure Catalogue (GLSSC; Alpaslan et al. 2014a,b). This catalogue has an absolute magnitude limit of $M_r = -17.6 + 5 \log h$ mag out to $z = 0.09$; these limits are chosen such that the catalogue is complete to a stellar mass of $\geq 9 \log M_*/h^{-2}\,M_\odot$. Classification of galaxies as belonging to three types of large-scale environments (filaments, tendrils and voids) was performed on this catalogue via a modified minimal spanning tree (MST) algorithm (Alpaslan et al. 2014a). Galaxy groups from Robotham et al. (2011) are first used as nodes of an MST to find filaments; groups are considered to be in a filament if they are a distance b from each other, similar to a friends-of-friends algorithm. Galaxies that are a distance r from these filaments (or in a group in a filament) are defined as galaxies in filaments. All galaxies in filaments are then removed from the sample, and a second MST is generated on the remaining population. The second pass identifies tendrils, and any galaxy beyond a distance q from a tendril is considered to be an isolated void galaxy. The distances r and

q are chosen such that the two-point correlation function $\xi_2(r)$ of void galaxies is minimized. b is chosen such that at least 90 per cent of groups with $L \geq 10^{11}\,L_{\odot}$ are in filaments. For other examples of MST-based structure finders, see Doroshkevich et al. (2004) and Colberg (2007). The GLSSC is generated with $b = 5.75\,h^{-1}$ Mpc; $r = 4.12\,h^{-1}$ Mpc; and $q = 4.56\,h^{-1}$ Mpc. The catalogue used for this work is generated with $b = 3.7\,h^{-1}$ Mpc; $r = 3.79\,h^{-1}$ Mpc; and $q = 4.35\,h^{-1}$ Mpc.

An alternative filament finding algorithm based around the tidal tensor prescription has recently been used on GAMA data by Eardley et al. (2015). The tidal tensor methodology differs significantly from the MST approach used to generate the GLSSC, in that it is a density-based method that categorises volumes as belonging to knots, sheets, filaments or voids. Eardley et al. (2015) present a comparison of their galaxy classifications to the GLSSC in their appendix, and find that the two catalogues are in excellent agreement, particularly when it comes to categorizing galaxies as being in filaments. Such an agreement indicates that both methodologies are able to identify filamentary structures consistently: 92.6 per cent of GLSSC filament galaxies are in sheets, filaments, and knots defined by the tidal tensor method, with the majority (44.3 per cent) being filament–filament matches. For further details we refer the reader to appendix C and figs C1 and C2 of Eardley et al. (2015). A more comprehensive review and comparison of how a number of filament finding methods, including the MST algorithm used for the GLSSC, perform when run on the same data set will be presented by Libeskind et al. (in preparation).

2.2 Spiral galaxy selection

As mentioned in the Introduction, this work focuses exclusively on spiral galaxies that are in filaments. We vet against spheroidal galaxies, as their stellar population is influenced by a different set of dynamics within filaments (Tempel et al. 2014), as well as by local dynamical effects such as tidal forces and galaxy interactions, influenced by halo mass; these are all known to directly influence the SFR of a galaxy (Robotham et al. 2013). Concentrating on spiral galaxies, whose SFRs are related to the properties of their surrounding intergalactic medium (IGM; Grootes et al., in preparation), and selecting those which do not belong to groups or pairs, provides us the means to investigate whether galaxies have actively changing stellar populations influenced by their position along a filament.

Formally, this criterion means a selection of spiral galaxies that are within $r = 3.79\,h^{-1}$ Mpc from a filament, consistent with the maximum allowed distance between a galaxy and a filament as described in the preceding subsection. Furthermore, we only consider spiral galaxies that meet both this distance criterion and are not members of groups or galaxy pairs; this ensures a selection of isolated galaxies without satellites; this constitutes about 25 per cent of all spirals in filaments. Group membership information is taken from the Robotham et al. (2011) catalogue, and a galaxy is considered to be in a pair if it has a companion within a physical projected separation of $100\,h^{-1}$ kpc and a velocity separation of 1000 km s^{-1}. Our isolated galaxies are therefore considered to be isolated down to GAMA's detection limit of $m_r = 19.8$ mag. The accuracy of these group and pair classifications has been independently verified (Alpaslan et al. 2012), and benefits from GAMA's high target density and spectroscopic completeness, ensuring that our isolation criteria for our sample is very robust. By excluding such paired and grouped galaxies, one can study the stellar mass growth of spiral galaxies whose stellar populations and SFRs are not affected by processes

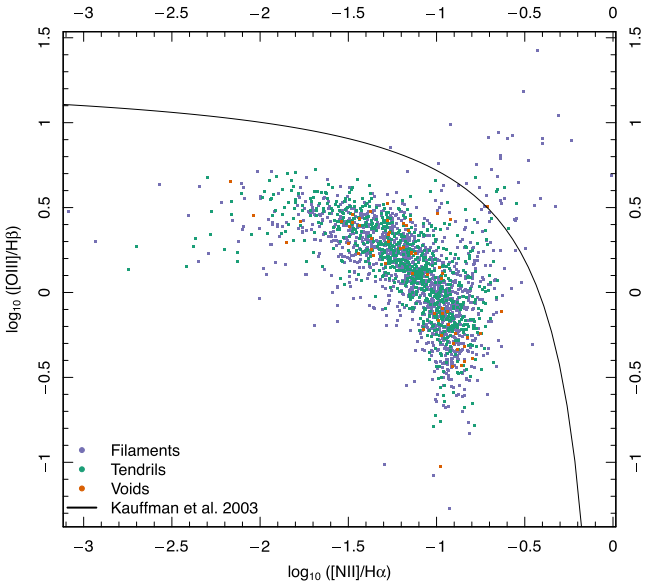

Figure 1. BPT diagram displaying the Kauffmann et al. (2003) relation, distinguishing star-forming galaxies from AGN/composite objects, for spiral galaxies in filaments, tendrils and voids (blue, green and orange, respectively). We reject all galaxies lying above the line as non-star formers.

that typically affect star formation in groups and pairs (e.g. Ellison et al. 2008; Robotham et al. 2013; Davies et al. 2015).

We identify spiral galaxies using the non-parametric, cell-based methodology described in Grootes et al. (2014), where combinations of two or three photometric parameters are used to divide populations of galaxies into morphological type. Morphological classifications from Galaxy Zoo Data Release 1 (Lintott et al. 2011) are used to calibrate this division. For each parameter combination, the space occupied by spiral galaxies identified from the Galaxy Zoo data set is divided into a series of cells whose sizes depend on local density of points. A given combination of parameters is judged to be successful at identifying spiral galaxies if a sufficient fraction of galaxies in these cells are indeed galaxies identified as spirals from Galaxy Zoo. A number of parameter combinations are found to perform well, and for this work we utilize the combination of $\log(n)$, $\log(r_e)$ and M_i, where n, r_e and M_i are the Sérsic index, effective radius and the i-band absolute magnitude of each galaxy. Sérsic indices and effective radii for each galaxy are taken from Kelvin et al. (2012). We additionally reject 45 non-star-forming galaxies as per the Kauffmann et al. (2003) BPT relation, displayed in Fig. 1. Line strengths in Fig. 1 are directly measured from GAMA spectra in a manner similar to that described in Gunawardhana et al. (2013) using MPFITFUN,[1] but with additional error modelling for each spectral fit. Our final sample contains 1799 star-forming spiral galaxies across the three equatorial GAMA fields, whose morphologies have been verified by independent visual inspection. An overhead view of these galaxies, as well as the overall filamentary structure that they reside in is shown in Fig. 2.

2.3 UV-derived SFR measurements

The SFR measurements provided in this paper are based on UV emission, corrected for Galactic and internal dust attenuation. Not only does the NUV provide an estimate of the SFR of a galaxy on

[1] http://www.physics.wisc.edu/craigm/idl/fitting.html

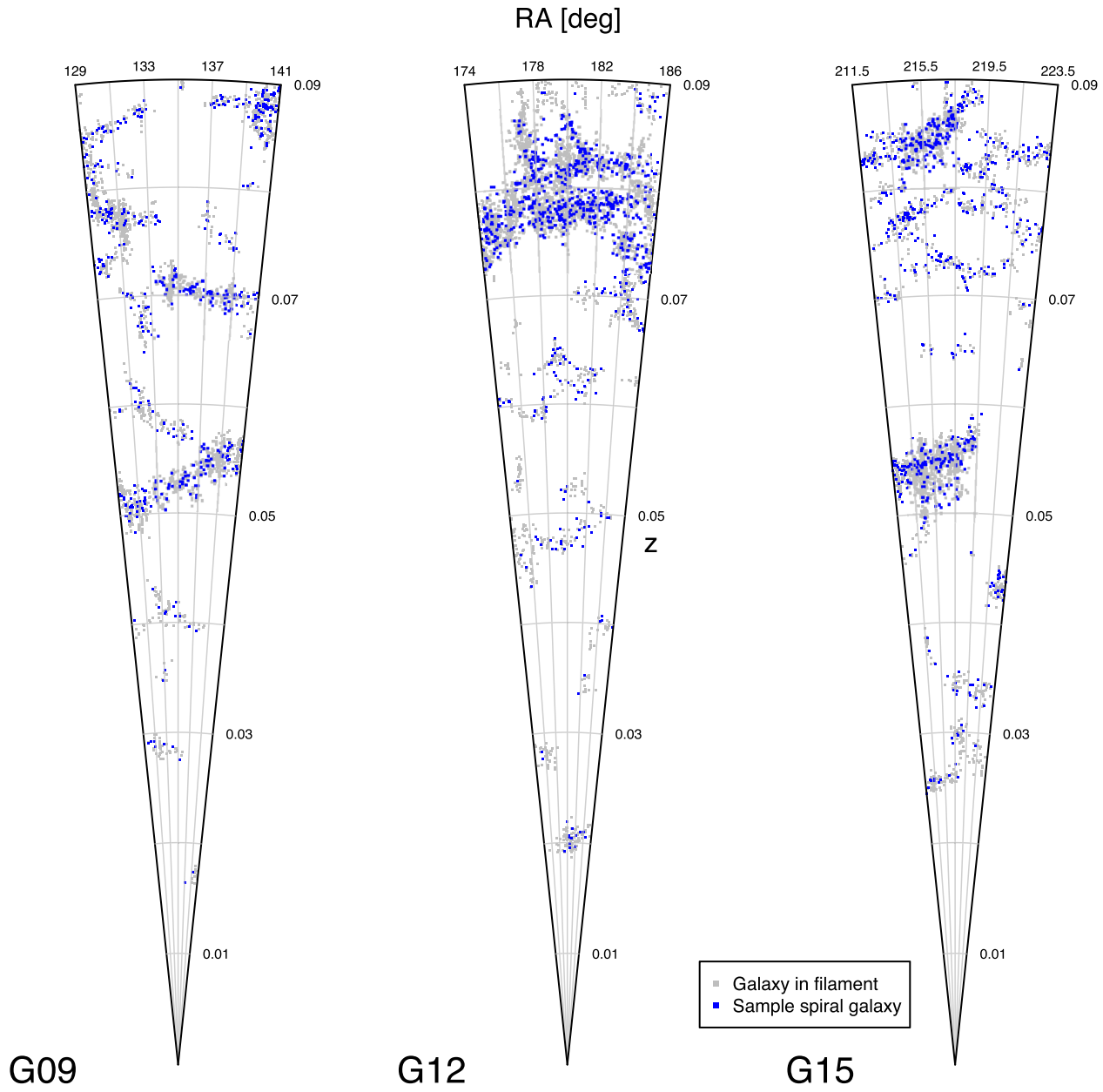

Figure 2. Overhead view of the three equatorial GAMA fields, with all filament galaxies in the low-redshift large-scale structure catalogue shown as grey points. Of those, non-AGN spiral galaxies that are not in groups or pairs are shown as blue points.

the time-scale of $\sim 10^8$ yr,[2] the GAMA NUV measurements also provide robust estimates of the total NUV flux, and accordingly the total SFR.

Coverage of the GAMA fields in the NUV is provided by *GALEX* in the context of *GALEX* MIS (Martin et al. 2005; Morrissey et al. 2007) and by a dedicated guest investigator programme (*GALEX*-*GAMA*), providing a largely homogeneous coverage to ∼23 mag. Details of the GAMA UV photometry are provided in Andrae et al. (in preparation), Liske et al. (2015) and on the *GALEX*-GAMA website.[3] Briefly however, extraction of UV photometry proceeds as follows: GAMA provides a total of three measurements of NUV fluxes. First, all *GALEX* data are processed using the *GALEX* pipeline v7 to obtain a uniform blind source catalogue[4] with a signal-to-noise (S/N) cut at 2.5 σ. This catalogue has subsequently been matched to the GAMA optical catalogue using an advanced matching technique which accounts for the possibility of multiple matches between optical and NUV sources, redistributing flux between the matches as described in Andrae et al. (in preparation) and on the *GALEX*-GAMA website. Additionally NUV photometry at the positions of all GAMA target galaxies is extracted using a curve-of-growth algorithm, as well as apertures defined on the measured

[2] For a galaxy with a constant SFR the rest-frame luminosity-weighted mean age of the *GALEX* NUV filter is $\sim 10^8$ yr (Gilbank et al. 2010, Grootes et al., in preparation).

[3] www.mpi-hd.mpg.de/galex-gama/

[4] The band merged *GALEX* blind catalogue is *NUV*-centric, i.e. *FUV* fluxes have been extracted in *NUV* defined apertures, entailing that no catalogued source can be detected only in the *FUV*.

size of the source in the *r*-band. For one-to-one matches preference is given to the pipeline photometry, while for extended sources and multiple matches, the curve-of-growth and aperture photometry is preferred. The resulting best estimates of the total NUV flux of the galaxy is reported as BEST_FLUX_NUV, in the UV photometric catalogue. In the work presented here, we have made use of these estimates applying galactic foreground extinction corrections following (Schlegel, Finkbeiner & Davis 1998),[5] and k-corrections to $z = 0$ using KCORRECT_V4.2 (Blanton & Roweis 2007).

The determination of the SFR of a galaxy from its NUV emission requires *intrinsic* emission which has been corrected for the attenuation of the stellar emission due to the dust in the galaxy, which is particularly severe at short (UV) wavelengths (e.g. Tuffs et al. 2004). Our analysis is focused on the differential effects in the SFR of spiral galaxies as a function of (large-scale) environment. However, both the so-called main sequence of star-forming galaxies (e.g. Noeske et al. 2007; Whitaker et al. 2012) as well as work on the SSFR – stellar mass relation for purely morphological samples of spiral galaxies (Grootes et al. 2014, Grootes et al., in preparation) imply that environmental effects are likely of second order and superimposed on the dominant influence of galaxy properties such as stellar mass. Accordingly, we require a method of obtaining accurate attenuation corrections which is as free as possible of both systematic and random errors.

In this paper we have adopted the method of Grootes et al. (2014) which uses the radiation transfer model of Popescu et al. (2011), and supplies attenuation corrections on an object-by-object basis for spiral galaxies, taking into account the orientation of the galaxy in question. As demonstrated by Grootes et al. (2014) the optical depth due to dust, critically determining the attenuation of emission from a galaxy, can be estimated using the effective stellar mass surface density μ_*, thus enabling the determination of highly accurate attenuation corrections for large samples of galaxies on an object-by-object basis. In determining attenuation corrections we have proceeded as follows.

The GAMA measurements of galaxy stellar mass and size have been used to determine the effective stellar mass surface density μ_* as

$$\mu_* = \frac{M_*}{2\pi D_A^2(z)\theta^2_{e,\mathrm{ss},r}}\ , \tag{1}$$

where $D_A(z)$ is the angular diameter distance corresponding to the redshift z, M_* is the stellar mass and $\theta_{e,\mathrm{ss},r}$ is the angular size corresponding to the effective radius of the *r*-band single Sérsic profile. Subsequently, μ_* is used to estimate the optical depth, which combined with a measurement of the inclination of the galaxy, is used to predict the attenuation in the UV-optical bands using the model of Popescu et al. (2011). The reader is referred to Grootes et al. (2014) for further details of the process and the Popescu et al. (2011) model.

Using the intrinsic absolute foreground extinction corrected NUV magnitudes derived in this manner we estimate the SFR using the conversion given in Kennicutt (1998) scaled from a Salpeter (1955) IMF to a Chabrier (2003) IMF as in Salim et al. (2007), i.e.

$$\mathrm{SFR}[\,\mathrm{M_\odot yr^{-1}}] = \frac{L_{\mathrm{NUV}}[\mathrm{Js^{-1}Hz^{-1}}]}{1.58 \times 7.14 \times 10^{20}} \tag{2}$$

The SSFR ψ_*, the SSFR, is computed by dividing the SFR for each galaxy by its stellar mass M_*. GAMA stellar masses are calculated from synthetic spectra fit to rest-frame *ugriz* photometry for each galaxy, see Taylor et al. (2011) for further details. For two galaxies in our sample this process yields unphysically high SFR estimates due to poor size estimates. These errors lead to an overestimation of their dust content, and consequently an overattenuation of their UV flux. These two galaxies are committed from the subsequent analysis in this paper. We show the relationship between stellar mass and SFR[6] for these selected filament galaxies in Fig. 3.

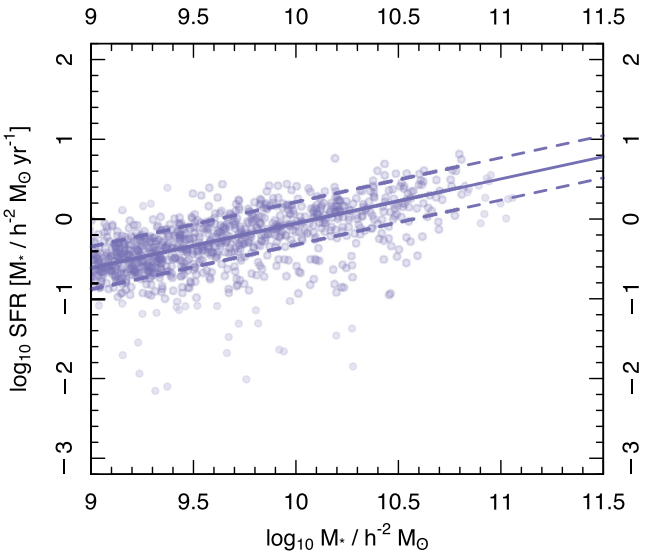

Figure 3. SFR as a function of stellar mass for ungrouped, unpaired, non-AGN spiral galaxies in filaments. The model fit to the data is shown as the solid line, with 1σ contours shown as the dashed lines above and below the median.

2.4 Distance metrics

Filaments, despite their relative linearity, are difficult structures to characterize geometrically, and this difficulty is further enhanced by the fact that filaments are made up of discrete particles (galaxies) as opposed to continuous distributions of matter. Further, objectively defining the 'centre' of a filament and the distance to that centre from a given galaxy are non-trivial tasks. For recent discussions on this particular issue, we refer the reader to Aragón-Calvo et al. (2010) and Cautun et al. (2014).

We build upon the work of structurally decomposing filaments that was presented in Alpaslan et al. (2014a), specifically in Appendix A. There, the centre of a filament is defined as the group that is furthest away from any of the edges of the filaments, within the structure imposed on it by the MST formed between its constituent groups. 'Furthest away' can be defined both in terms of physical 3D comoving distance between the groups, as well as simply the number of groups between the centre and the edge. In this work, the former definition is used. The longest continuous path of links from one end of the filament to another through the filament centre is defined as the first-order branch or backbone, and

[5] In the NUV we make use of $A_{\mathrm{NUV}} = 8.2\,E(B-V)$ as provided by Wyder et al. (2007).

[6] The line fitting in all figures is done using the HYPERFIT package (Robotham & Obreschkow 2015, http://hyperfit.icrar.org). HYPERFIT uses either downhill searches or MCMC (Markov chain Monte Carlo) methods to calculate the best-fitting parameters for a hyperplane of $D-1$ dimensions for D dimensional data. For this work we run HYPERFIT using its Nelder-Mead downhill simplex (Nelder & Mead 1965) implementation.

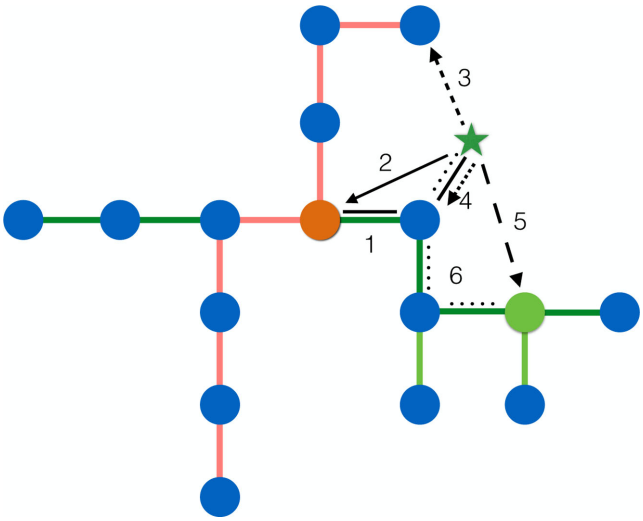

Figure 4. Schematic of a filament, with its constituent groups represented as large blue circles. The orange and green circles represent the central and most massive groups, and the star represents a hypothetical spiral galaxy within the filament. Links are coloured according to their branch order, with the backbone shown as the thick pink links. Second- and third-order branches are dark and light green, respectively. The six distance metrics we use are shown as different lines, and are numbered according to their description in Section 2.4.

represents the primary 'axis' of the filament. Paths that lead into the backbone are referred to as second-order branches. Generally, paths that lead into nth-order branches are referred to as $(n + 1)$th-order branches.

These considerations lead to 6 different ways to characterize the distance between spiral galaxies and the filaments that they reside in. The distance metrics fall into two broad groups: (1) direct radial distances between the spiral galaxy and different components of the filaments, e.g. the central group, and (2) distance travelling along the filament links from the spiral galaxy to different filament components. These two categories probe slightly different aspects of gas flow within filaments: the first is more sensitive to radial changes in the gravitational potential well of a filament and how that influences star-forming gas, while the second probes the transversal changes in gas properties as it travels along the links within a filament. Fig. 4 provides an overview of the metrics that we use in this work for an idealized two dimensional case. An interactive 3D model of a filament with these same distance metrics is shown in Fig. 5.

(i) The distance from the target galaxy to the central group of the filament, along the links in the filament. The radial distance from the galaxy to the nearest filament group is added to this. The central group is defined as the group that is furthest from any edge of the filament (see Alpaslan et al. 2014a);

(ii) the radial distance from the target galaxy to the central group of the filament;

(iii) the radial distance from the target galaxy to the nearest group in the backbone of the filament;

(iv) the orthogonal distance from the target galaxy to the filament;[7]

(v) the radial distance from the target galaxy to the most massive group in the filament, where mass is defined as the sum of the stellar mass of its constituent galaxies; and

(vi) distance by links from the target galaxy to the most massive group in the filament. As with the first metric, the radial distance to from the galaxy to the nearest filament group is also added to this.

3 STELLAR CONTENT ALONG THE COSMIC WEB

3.1 Filaments

For each galaxy in our sample, we compute its distance relative to its filament according to the six metrics described in the preceding section. To avoid recovering star formation trends driven by stellar mass instead of filament morphology, we compute an SSFR offset value for each galaxy, similar to Grootes et al. (in preparation). We begin by calculating median values of SSFR (ψ) in bins of stellar mass for the sample shown in Fig. 3, and interpolating between them. The interpolated relation is fit by the line $y = -0.35x - 6.54$. Each galaxy's SSFR offset is then defined as $\psi_{\rm galaxy} - \psi_{\rm med}$, where $\psi_{\rm med}$ is a median SSFR value calculated for the stellar mass of that particular galaxy from our interpolated medians; errors in star formation are included in each fit.

We perform linear fits to the data for each metric, and find that in most cases, the errors are consistent with the slope of the fit being zero. To ensure that a linear fit is most appropriate, we compute Bayesian information criteria (Schwarz 1978) for linear and polynomial fits and find that the BIC for a linear model is lowest by a margin of $\Delta{\rm BIC} > 10$. For the distance metric that measures the orthogonal distance between the galaxy and the filament we detect a very faint upward slope of 0.031 ± 0.008, which is shown in Fig. 6. The remaining fits are included at the end of this paper, in Fig. 14. In both figures, the fit is shown as the solid line, with 1σ errors in the fit represented by the dashed lines. The trend in this figure is statistically significant at a 3σ level and is consistent with a very subtle enhancement of SSFRs for galaxies closer to voids (i.e. on the outer edge of a filament) compared to those near the cores of filaments. A number of different scenarios may explain this relationship: galaxies on the peripheries of filaments are more exposed to gas, which is subsequently used to fuel new star formation; gas at the core of a filament is hotter than at the peripheries, and therefore more difficult to accrete; or galaxies travelling from the periphery of a filament to its core may simply be using up their gas reservoirs. These scenarios are all explored in greater detail in the Discussion section. As a way of checking if signals in other distance metrics are washed out at long distances, we have repeated this calculation and considered only galaxies within 5 h^{-1} Mpc of the filament for each distance metric; as well as fitting jackknife resampled distributions (where we reject a random 10 per cent of galaxies for each iteration), and our results remain unchanged.

We also track stellar mass in these galaxies as a function of our distance metrics. Once again there are no statistically significant trends in stellar mass as a function of most of the distance metrics except for the orthogonal distance to the filament, which is shown in Fig. 7, while the full set of fits is at the end of the paper, in Fig. 15. Here there is a statistically significant slope of -0.058 ± 0.018, indicating that galaxies closer to the edges of filaments have lower

[7] This distance metric is originally defined in Alpaslan et al. (2014a), where it was used to determine if a galaxy was close enough to a filament to belong to it. For a given galaxy, the distance to the filament is defined as the radial distance between the galaxy and the nearest filament group or filament link, depending on which is the shortest.

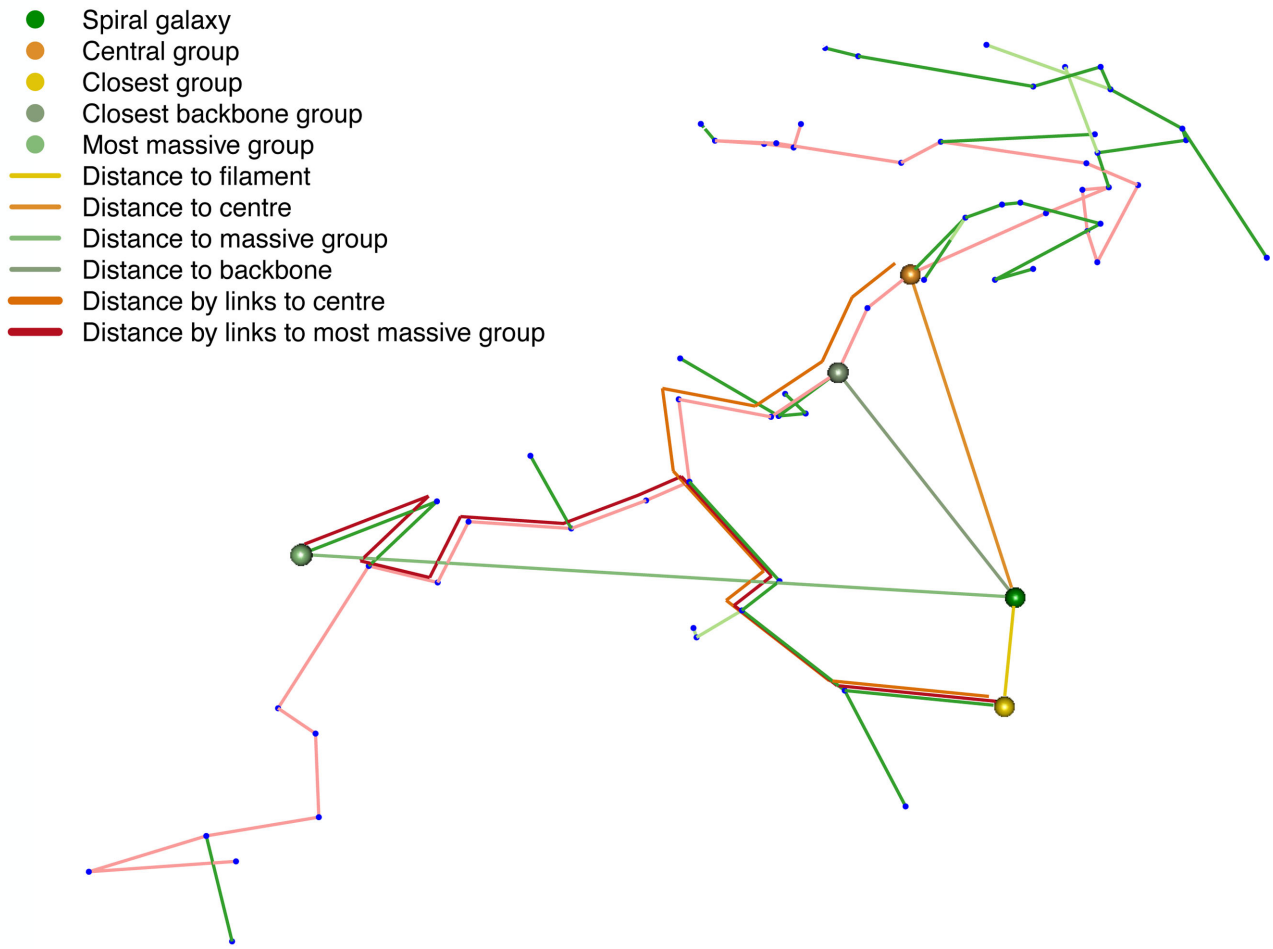

Figure 5. A 3D, interactive model of a filament, and a spiral galaxy within it. If the figure does not appear interactive, please view with a current version of Adobe Reader. The filament is represented as a series of links that connect its constituent groups, which are shown as blue cubes. The links are coloured according to their rank, i.e. the backbone links are shown as pink lines, and second- and third-order branches are shown as green and light green lines. The spiral galaxy, central group, closest group, closest backbone group and most massive group are shown as green, orange, yellow, grey and teal; and the lines representing the distances to those groups are shown in matching colours. Finally, the distance by links to the central group and most massive group are shown as red and burgundy lines, offset from the filament links. Views for the interactive figure showing all of these components may be accessed from the toolbar at the top of the interactive figure, and the 3D figure can be viewed as a separate window by selecting the relevant option from the contextual menu.

stellar masses than those in the cores; this is in good agreement with the recent work of Chen et al. (2015). Given that our sample consists of galaxies outside of groups and pairs, this rise in stellar mass is unlikely due to be caused by local environmental effects (i.e. galaxy–galaxy interactions within groups and pairs). Coupled with the trend seen for the same distance metric in Fig. 6, these two figures indicate that galaxies on the peripheries of filaments are forming stars more efficiently despite having lower masses, while those at the cores of filaments are heavier and forming fewer stars.

We check against the possibility that these effects are simply caused by the local density of our sample galaxies by plotting the SSFR offset and stellar masses of galaxies as a function of their local density, using the `EnvironmentMeasuresv03` catalogue of Brough et al. (2013), where local densities are calculated for all GAMA galaxies. The surface density of each galaxy is calculated based on the distance to its fifth nearest neighbour within a velocity cylinder of $\pm 1000\,\mathrm{km\,s^{-1}}$, and are corrected for survey completeness. These are shown in Figs 8 and 9. We find that neither the SSFR offset, or the stellar mass of our sample galaxies depend at a statistically significant level on their surface densities, providing further indication that the effects seen in Figs 6 and 7 are driven by large-scale structure.

3.2 Comparison to tendrils and voids

We complement our initial sample of 1799 unpaired and ungrouped spiral galaxies in filaments with an additional 946 and 67 in tendrils and voids, respectively; in both cases the spiral galaxies are also star forming, ungrouped and unpaired (hereafter these galaxies are referred to as the combined LSS sample). The calculation of the SSFR offset for the tendril and void populations is done in the same way as for the filaments, as described in Section 3.1. We further subdivide these galaxies by their stellar mass into two bins, above and below their respective population medians (9.5, 9.43 and 9.25 $\log M_*/h^{-2}\,\mathrm{M}_\odot$ for filaments, tendrils and voids, respectively). We show these distributions in 10, where in each panel SSFR offsets are shown by environment for galaxies above and below their populations' median stellar mass, with the median of each

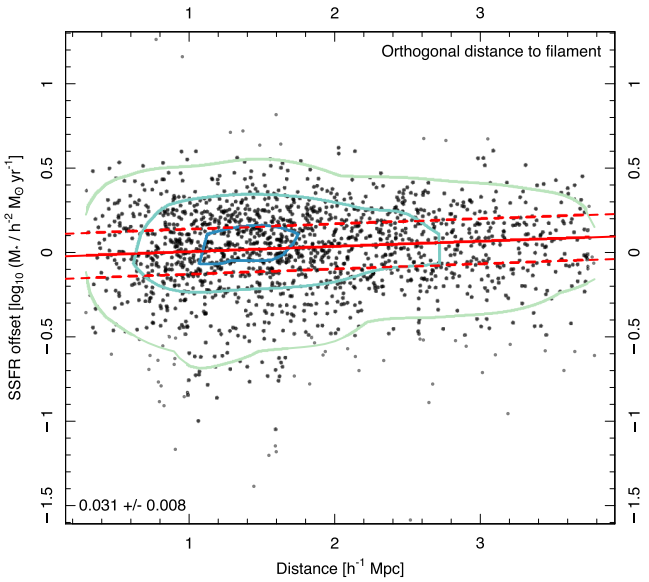

Figure 6. Offset in UV-derived SSFRs of spiral galaxies in filaments as a function of their orthogonal distance to their host filament. The solid lines show fits to the data using the HYPER.PLANE fitting package Robotham & Obreschkow (2015), and the dashed lines represent 1σ errors on the fit. Coloured contours show the 90th, 50th and 10th percentiles of data, respectively. The gradient and associated error for the fit is shown in the bottom left. The fit indicates that the SFRs of spiral galaxies in filaments are higher closer to the edge of the filament when compared to the core of the filament. The detection of such an effect in ungrouped and unpaired spiral galaxies means that the most likely explanation for this change in SFRs is a change in the availability of gas to these galaxies as a function of their orthogonal distance to the filament core.

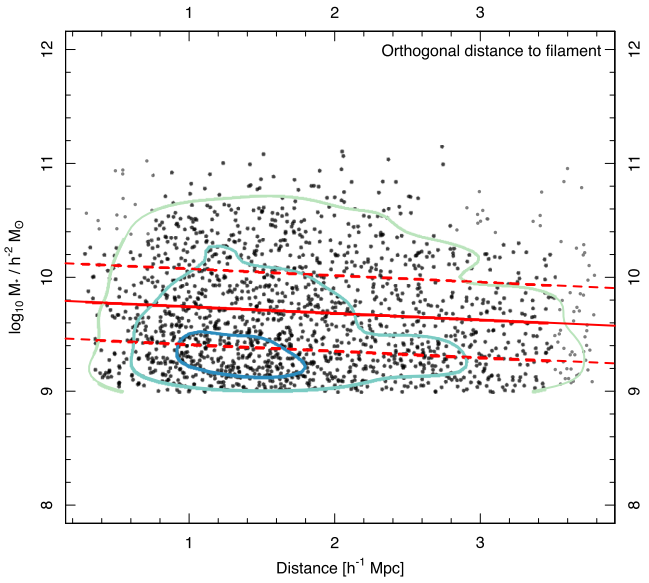

Figure 7. Stellar masses of spiral galaxies in filaments as a function of orthogonal distance to their host filament. The line fits in this figure are done in the same way as those in Fig. 6. Coloured contours show the 90th, 50th and 10th percentiles of data, respectively. We detect a statistically significant downward trend in stellar mass as a function of orthogonal distance to the filament, showing that the stellar mass of spiral galaxies rises towards the core of a filament, and drops at its outer edges.

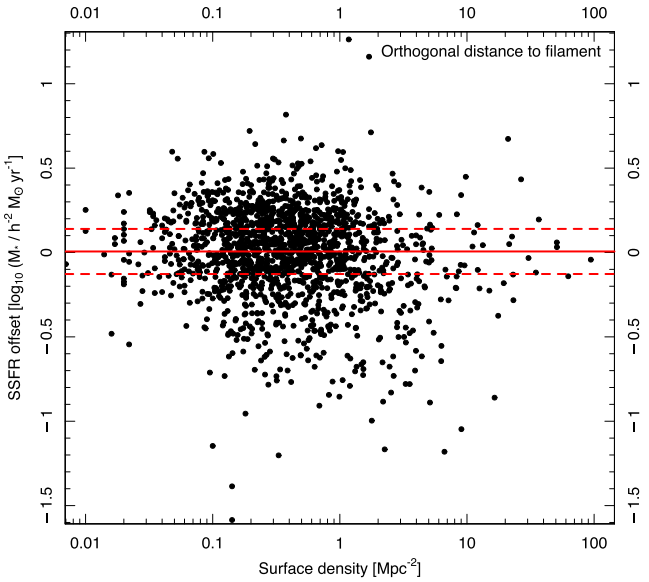

Figure 8. Surface density as defined by the five nearest neighbours of each galaxy from Brough et al. (2013) as a function of SSFR offset for filament spiral galaxies. We detect no statistically significant correlation between these two parameters.

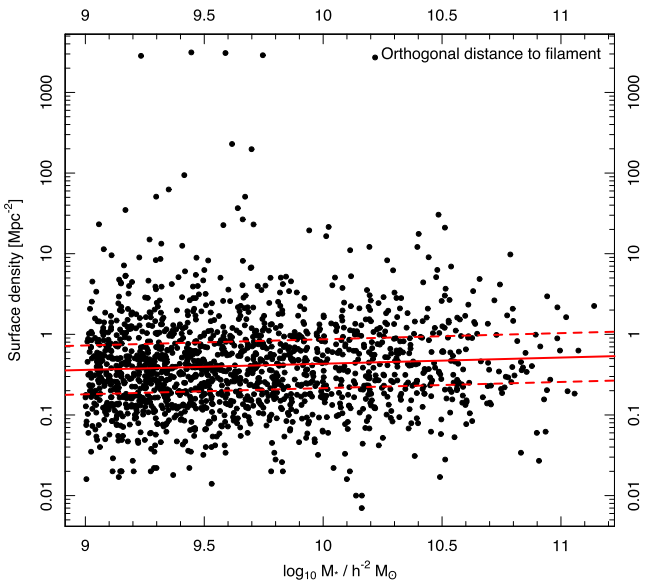

Figure 9. Stellar mass as a function of surface density as defined by the five nearest neighbours of each galaxy from Brough et al. (2013) for filament spiral galaxies. We detect no statistically significant correlation between these two parameters.

distribution and its standard error represented by the vertical line and shaded region in the corresponding colour. All three populations display very similar trends in SSFR offset; this result indicates that large-scale structure does not greatly impact the overall SFRs of spiral galaxies.

Here we highlight the peculiar bimodality in SSFR offset seen for low-mass void galaxies (as seen in the bottom panel of Fig. 10); this appears to be a sub-population of low-mass galaxies that have strikingly low SFRs. A jackknife resampling of the void galaxy sample confirms that this distribution is statistically significant. Visual inspection of these galaxies does not present an explanation for

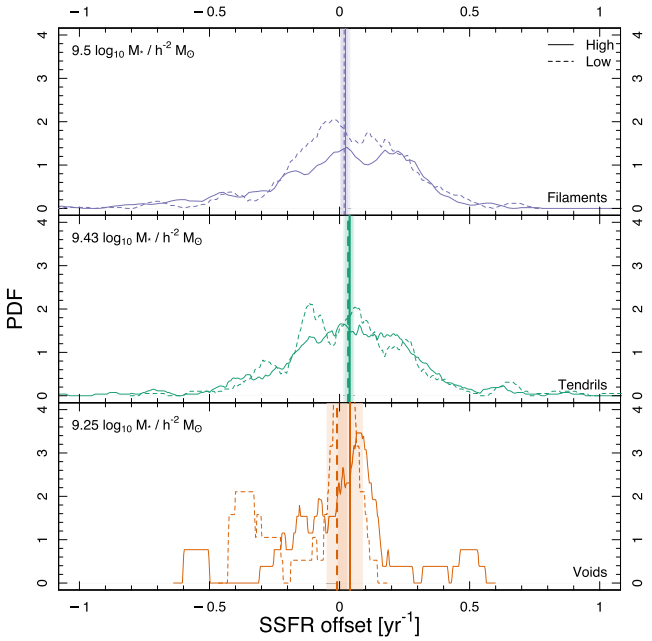

Figure 10. SSFRs of spiral galaxies in different environments, subdivided into populations of low and high stellar mass (shown as dashed and solid lines, respectively), with PDFs calculated by convolving the data with a rectangular kernel of bandwidth 0.1 dex. The vertical lines represent the median SSFR value for that population, and the shaded area shows the standard error on the median. While there is a small tendency for the SSFR of low-mass galaxies to be higher in voids, the effect of stellar mass is greater than that of large-scale environment. The median mass for each population, which divides the high- and low-mass sub-samples, is shown in the top left.

their lower SFRs; nor are they physically clustered together. We display these galaxies in Fig. 11, where we present the three equatorial GAMA fields as in Fig. 2, this time highlighting our sample of void spiral galaxies in red. The sub-population of low-mass star-forming void galaxies are shown in black boxes.

The relative unimportance of large-scale structure in the SFRs of spiral galaxies is also shown in Fig. 12, where we plot SFR as a function of stellar mass for each galaxy in our combined LSS sample. As we show in Figs 10 and 12, the median SSFR shows very little to no dependence on large-scale structure. However, the distributions indicate that environment may nevertheless play a secondary impact in terms of broadening the distribution, as seen in Figs 10 and 13. In the latter plot the variance in SFR as a function of stellar mass for galaxies in filaments, tendrils and voids is shown. Galaxies in voids are shown to have a more narrow spread of SFRs in each stellar mass bin. In Fig. 12 we also show, as black crosses, the population of void galaxies that generates the low-mass, low-SSFR offset in Fig. 10. These low-mass void spiral galaxies, while small in number, are forming far fewer stars than other void galaxies, and may represent a secondary mass-SFR main sequence for this population of galaxies. Environment does appear to play a role in the spread of SFRs for a given mass bin, however.

4 DISCUSSION

In this work we have sought out trends in SFR and stellar mass as a function of distance from a filament for a sample of ungrouped and unpaired spiral galaxies using data from the GAMA survey. Additionally, we have considered the instantaneous star formation of spiral galaxies in voids and tendrils contrasting these environments with the filament galaxies in our main sample. Furthermore, by making use of a mass complete morphologically selected sample as well as highly precise and accurate SFR measurements in the analysis presented in this work we have been able to quantify the subtle environmental dependencies in SFR at fixed stellar mass. This analysis has lead to a number of novel results which we will discuss in more detail below.

(i) Spiral galaxies at the edges of filaments, on the borders of voids, have higher SSFRs (at fixed stellar mass), and lower stellar masses compared to their counterparts at the cores of filaments. Specifically, our results indicate that spiral galaxies at the peripheries of filaments have greater access to reservoirs of star-forming gas compared to their counterparts in the cores of filaments.

(ii) Although the median relation between SFR and stellar mass is similar for filament, tendril and void spiral galaxies, the width of the distributions increases from voids to tendrils and filaments.

4.1 Star formation in filaments

To investigate the impact the large-scale structure (in the form of filaments) has on (spiral) galaxies we considered the UV-derived SSFR of these galaxies as a function of their position relative to the surrounding large-scale structure, i.e. their host filament using 6 different distance metrics (Fig. 6). Of these we find a statistically significant trend in SSFR with position for one: the orthogonal distance to the filament, which is shown in Fig. 6. A corresponding trend is found for the stellar mass of the galaxies, with galaxies closer to the cylindrical core being found to be more massive on average (Fig. 7). Our results therefore indicate that spiral galaxies close to the cylindrical core of a filament have a very slight tendency to have lower SSFRs and higher stellar masses. When comparing the median SSFR–M_* relations for spiral galaxies in filaments voids and tendrils in Fig. 12, however, we find no significant difference. This result confirms the findings of Alpaslan et al. (2015) and Grootes et al. (in preparation) that stellar mass plays a decisive role in determining galaxy properties, and that environmental effects such as those arising from the large-scale structure are second-order perturbations on this dominant trend.

The observed changes in stellar populations for these spiral galaxies as a function of their position with respect to a filament may be caused by a number of different physical processes. At a fundamental level, however, in order to support star formation at the observed level for extended periods, spiral galaxies must accrete gas from their surrounding IGM in order to replenish the interstellar medium consumed by star formation (as well as that lost to outflows from the galaxy).

For isolated galaxies at the centre of haloes with $M_{\rm halo} \lesssim 10^{12}\,{\rm M}_\odot$ Dekel & Birnboim (2006) have argued that this fueling predominantly takes the form of smooth cold flows of gas penetrating the virial radius of the DM halo to reach the galaxy, leading to the formation of a a disc and efficient star formation. Furthermore, recent work by Pichon et al. (2011), Codis, Pichon & Pogosyan (2015), Welker et al. (2015) indicates that the preferential directions for these cold flows are determined by the large-scale filamentary DM structure, with the filaments being fed by flows of gas from voids and walls, which is then advected on to the DM halo of the galaxy as a cold flow with high angular momentum, thus further spinning up the galaxy and supporting the disc.

The gas being accreted into the filament, however, is heated by the cylindrical shock surrounding the filament as well as by shocks within the filament. Furthermore, as recently demonstrated by

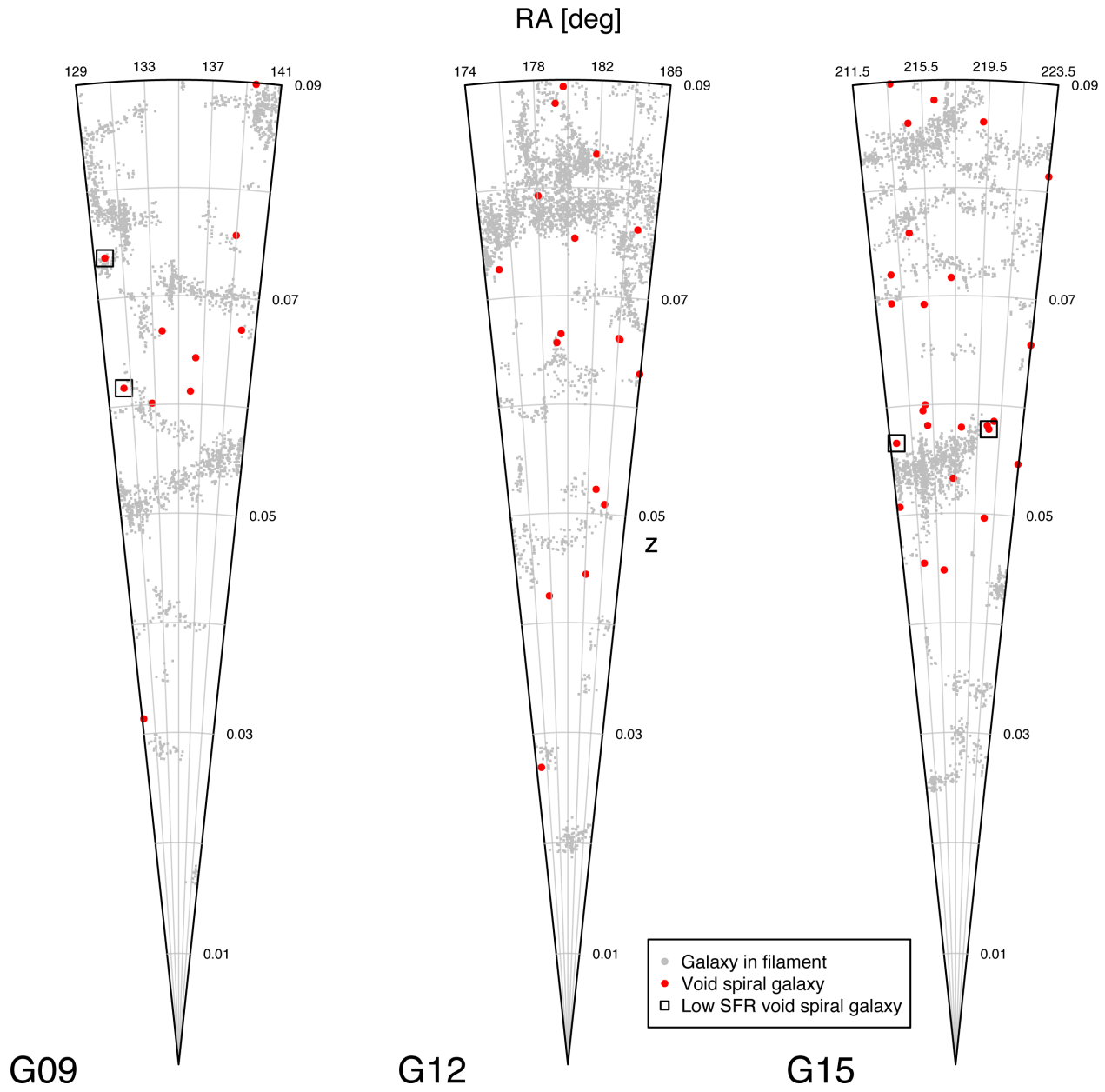

Figure 11. As with Fig. 2, but displaying the positions of the spiral galaxies in voids for our sample as red circles. Note that any void galaxy within 1° of the survey edge, as well as with $z > =0.085$ is not included in our analysis, as the large-scale structure classification of these galaxies as voids may not necessarily be accurate. Void spiral galaxies that constitute the low star-forming sub-population are shown in black squares.

Nelson et al. (2013) cool dense flows into a more diffuse hot medium may be efficiently heated and dispersed. Thus, the rate at which gas can be accreted on to a (spiral) galaxy in a filament will depend on (i) the degree to which the cold flows entering the filament retain their coherence and remain connected to the halo of the galaxy and (ii) the cooling time-scale of the shock-heated gas which depends sensitively on the temperature.

Numerical simulations of the IGM in and around filaments (Dolag et al. 2006; Zinger et al. 2015) find a denser but simultaneously hotter IGM in filaments, with both temperature and density increasing towards the centre, while at smaller scales the temperature of gas inside relaxed clusters decreases towards the cluster outskirts (Kravtsov & Borgani 2012). Furthermore recent work by Benítez-Llambay et al. (2013) suggests that low-mass haloes can have their gas stripped by ram pressure caused by the cosmic web. In combination, these trends may limit the inflow of accretable gas, providing a natural explanation for our empirical findings. With ongoing star formation in galaxies, such a scenario would also provide a natural explanation for the trend in stellar mass seen in Fig. 15. More detailed modelling and further observations will be necessary to investigate this scenario, though such work is beyond the scope of this paper.

Other possible explanations may be that the observed trends in SFR mirror the availability of gas to galaxies in filaments as a function of their position; these galaxies may simply be exposed to less gas with which to form stars, or are cut off from the resupply of gas and deplete their gas reservoirs as they migrate to the core of the filament (but see Grootes et al. (in preparation) for evidence that

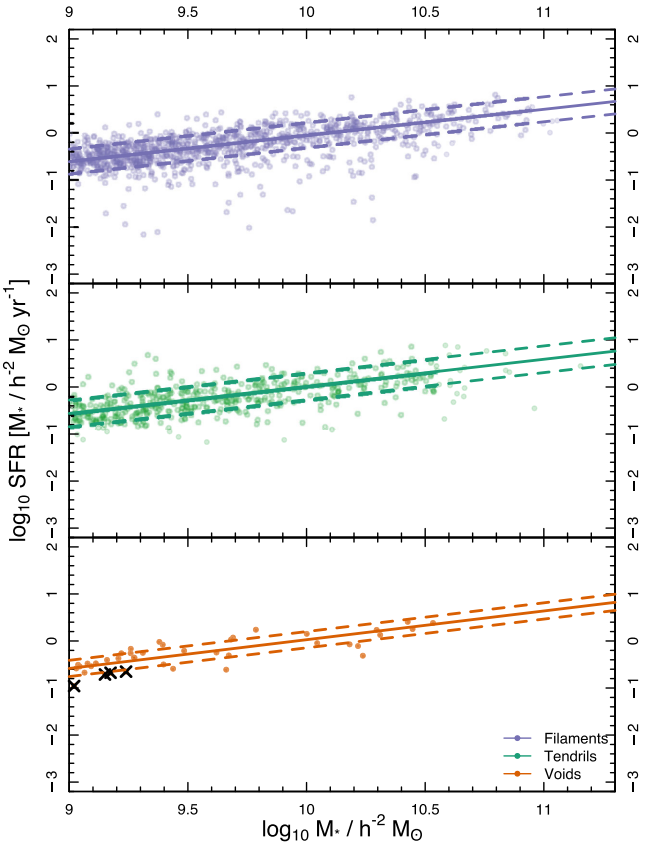

Figure 12. SFRs as a function of stellar mass for all galaxies in the combined LSS sample split by filaments, tendrils and voids (top, middle and bottom panels, respectively). Model fits to the data are shown for each population as solid lines in their respective colours, with dashed lines representing the 1σ contour to the model. Black crosses in the bottom panel represent the galaxies that form the low-mass, high-SSFR offset peak seen in Fig. 10. All three populations exhibit a similar SFR–M_* relationship.

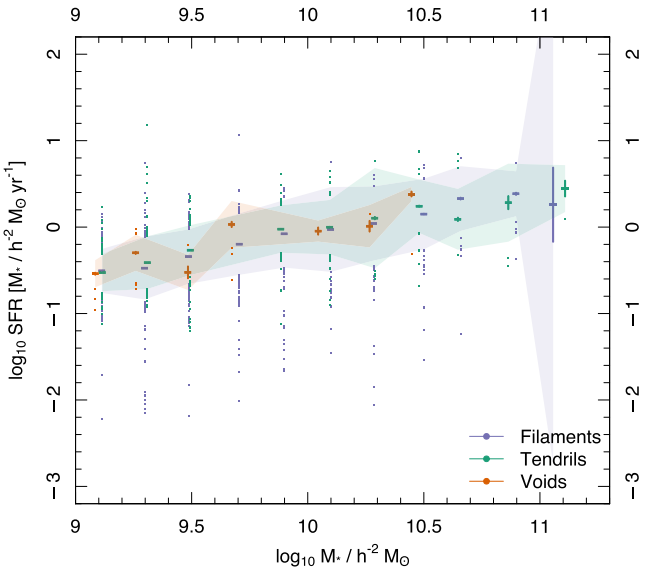

Figure 13. As with Fig. 12, but with data binned into stellar mass bins of 0.2 dex. For each bin we show the median and its standard error as the solid lines; the variance as the shaded region, and outlier data points beyond the variance as individual points.

this explanation is unlikely to be the case). Notably, in our analysis we have only found evidence for variations in the SFR and stellar mass perpendicular to the filament rather than along it. It seems likely that the gradient in the gravitational potential, and hence the accompanying changes in the thermodynamic properties or availability of the IGM is largest perpendicular to the filament. We must, however, also consider the possibility that our metrics struggle to capture the complex geometry of filamentary structures (evident in Figs 2 and 4), which will more severely impact metrics designed to trace this geometry over large distances (particularly those designed to follow links in the MST), causing a potential loss in signal. We are, further, only probing the properties of the IGM/flow of gas by tracking SFRs in spiral galaxies; ultimately, a detailed study of mass transport along the cosmic web will be rendered possible through the advent of next generation radio surveys to be conducted at the ASKAP, SKA or the MeerKAT.

4.2 Star formation in voids

As previously stated, and shown in detail in Figs 12 and 13, the average SFR–M_* relations for spiral galaxies in filaments, tendrils and voids are highly similar. However, as shown in Fig. 10 the distribution of SSFR around the relation at fixed stellar mass is much more peaked in voids than in filaments and tendrils. This difference may be taken to be indicative of the star formation histories in the former environment being much more uniform than in the other denser environments, where processes such as galaxy–galaxy interactions and different interactions of the galaxies with the changing surrounding IGM may lead to a diversification of the star formation history in comparison to the situation of void spiral galaxies, where star formation may be expected to be largely determined by the accretion of ambient IGM on to the host DM halo of the galaxy alone.

Finally, we note that for spiral galaxies in the mass range 10^9–$10^{9.5}$ $M_\odot$ in voids, one finds a clear bimodality in the distribution of SSFR with a small, but statistically significant secondary peak in the distribution offset to lower sFSR by 0.5 dex. Considering the positions of these sources on the SFR–M_* relation shown in Fig. 12, we find that this peak appears to trace a sequence parallel to that of the bulk of the void spiral galaxies, but offset towards lower star formation. Although the sample size is small, the observed bimodality remains robustly visible under jackknife sampling with a variation of sizes of the jackknifed sample. We therefore conclude the result to be robust in nature and physical. While the sample is too small in size for a more in depth analysis, we limit ourselves to drawing attention to the existence of this unexpected population of void spiral galaxies. We speculate that this feature may arise due to a more stochastic nature of star formation in the lowest mass galaxies, with the more diverse star formation history in higher density environments masking this effect in tendrils and filaments in the relevant stellar mass range.

5 SUMMARY

As expected, the stellar mass of a spiral galaxy plays a dominant role in determining its SFR. However, by making use of a sensitive analysis technique we have been able to identify environmental trends superimposed on this relation between star formation and stellar mass. In line with expectations based on the picture of large-scale

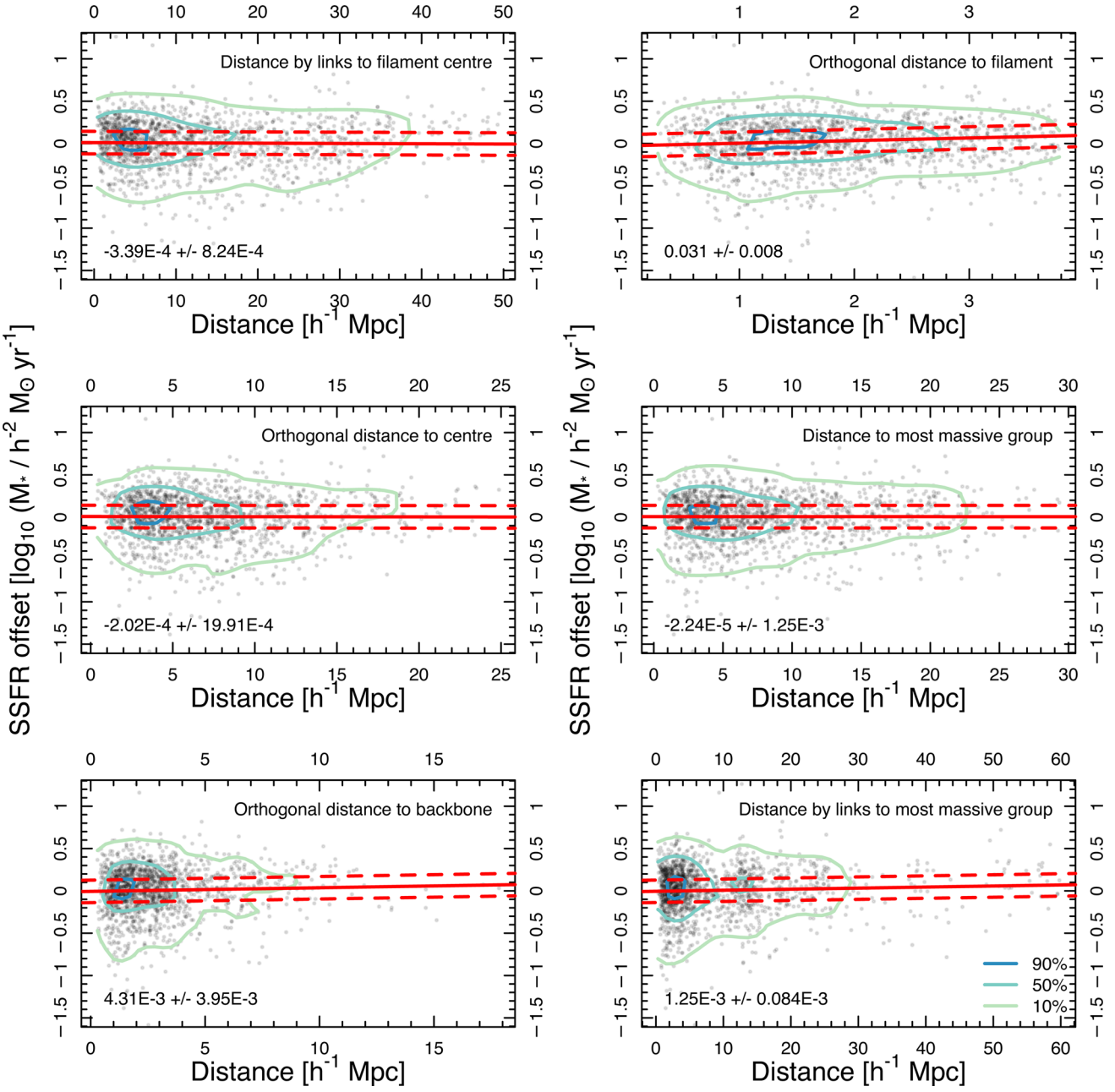

Figure 14. Offset in UV-derived SSFRs of spiral galaxies in filaments as a function of the six distance metrics described in Fig. 4, with data and fits shown as in Fig. 6. Aside from the orthogonal distance to the filament (top right), the gradients of the fits are statistically indistinguishable from being zero. The top-right panel is the only trend with a non-zero slope at a 3σ significance and indicates that the SFRs of spiral galaxies in filaments are higher closer to the edge of the filament when compared to the core of the filament. The detection of such an effect in ungrouped and unpaired spiral galaxies means that the most likely explanation for this change in SFRs is a change in the availability of gas to these galaxies as a function of their orthogonal distance to the filament core.

flows of gas on to filaments we find the SSFRs of spiral galaxies in filaments to be higher at fixed stellar mass on the periphery of the filament compared to its core, and also find the distribution of stellar masses of filament spiral galaxies to be skewed towards higher mass systems at the core. Extending our analysis to tendrils and voids, we have identified a significant bimodality in the distribution of SSFR of low-mass void spiral galaxies, which we speculate may be driven by the stochastic nature of star formation in these objects.

The results presented in this work must be considered as promising evidence for the complex interplay between galaxies and the cosmic web, as well as the influence of large-scale structure on galaxy evolution. They present a clear point of departure for future studies with new facilities and surveys capable of probing the relevant processes more directly and in greater detail.

ACKNOWLEDGEMENTS

MA is funded by an appointment to the NASA Postdoctoral Program at Ames Research Centre, administered by Oak Ridge Associated Universities through a contract with NASA. MALL acknowledges support from UNAM through the PAPIIT project IA101315. The

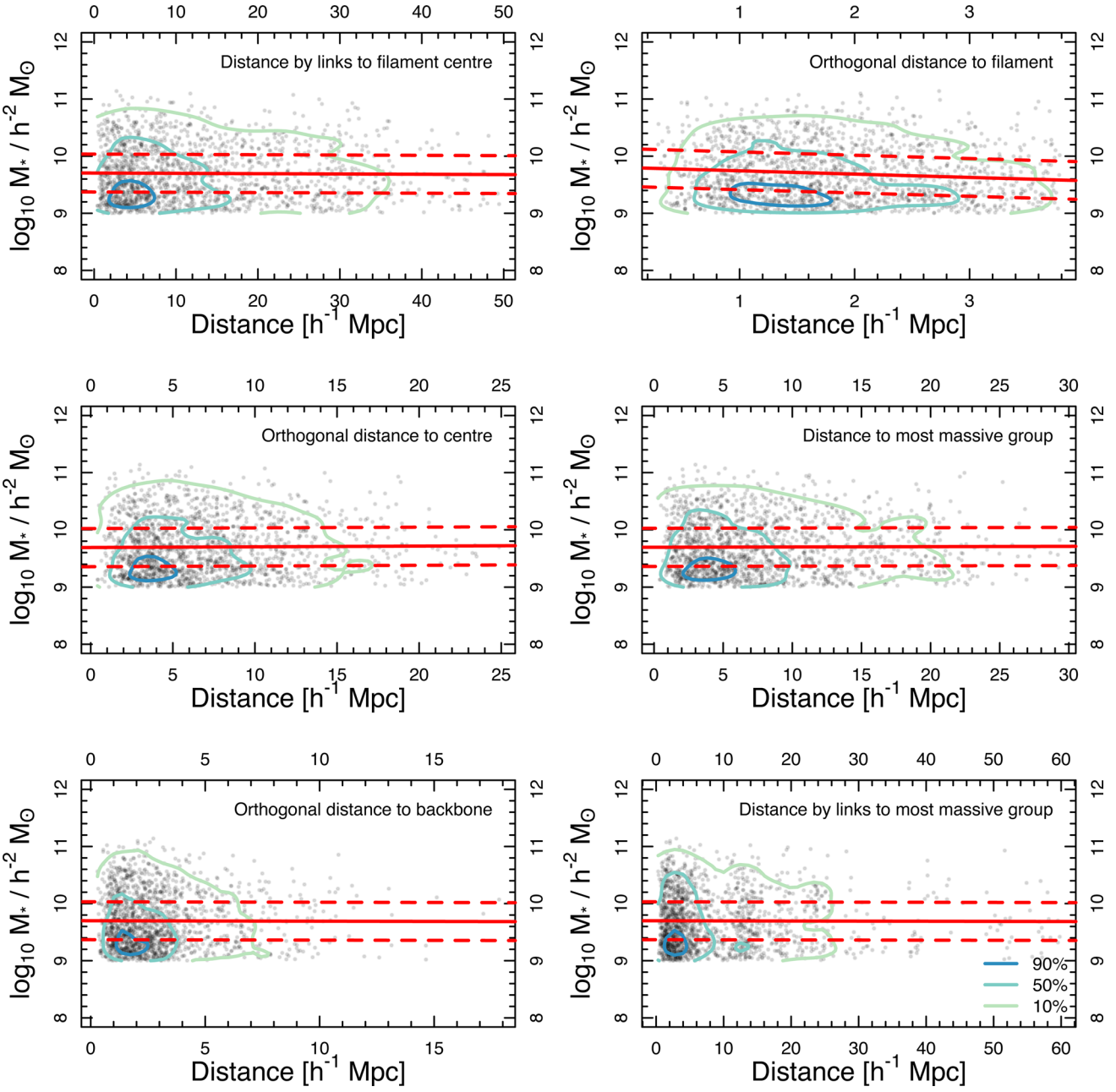

Figure 15. Stellar masses of spiral galaxies in filaments as a function of the six distance metrics described in Fig. 4, with data and fits shown as Fig. 7. We detect a statistically significant downward trend in stellar mass as a function of orthogonal distance to the filament (top-right), while all other fits are statistically consistent with having a gradient of zero.

authors would like to thank the anonymous referee, whose contributions have helped to improve this work.

GAMA is a joint European–Australasian project based around a spectroscopic campaign using the Anglo-Australian Telescope. The GAMA input catalogue is based on data taken from the Sloan Digital Sky Survey and the UKIRT Infrared Deep Sky Survey. Complementary imaging of the GAMA regions is being obtained by a number of independent survey programmes including *GALEX* MIS, VST KiDS, VISTA VIKING, *WISE*, *Herschel*-ATLAS, GMRT and ASKAP providing UV to radio coverage. GAMA is funded by the STFC (UK), the ARC (Australia), the AAO and the participating institutions. The GAMA website is http://www.gama-survey.org/. The VISTA VIKING data used in this paper are based on observations made with ESO Telescopes at the La Silla Paranal Observatory under programme ID 179.A-2004.

REFERENCES

Alpaslan M. et al., 2012, MNRAS, 426, 2832
Alpaslan M. et al., 2014a, MNRAS, 438, 177
Alpaslan M. et al., 2014b, MNRAS, 440, L106
Alpaslan M. et al., 2015, MNRAS, 451, 3249
Aragón-Calvo M. A., Jones B. J. T., van de Weygaert R., van der Hulst J. M., 2007, A&A, 474, 315
Aragón-Calvo M. A., van de Weygaert R., Jones B. J. T., 2010, MNRAS, 408, 2163

Benítez-Llambay A., Navarro J. F., Abadi M. G., Gottlöber S., Yepes G., Hoffman Y., Steinmetz M., 2013, ApJ, 763, L41
Blanton M. R., Roweis S., 2007, AJ, 133, 734
Bond J. R., Kofman L., Pogosyan D., 1996, Nature, 380, 603
Brough S., Forbes D. A., Kilborn V. A., Couch W., Colless M., 2006, MNRAS, 369, 1351
Brough S. et al., 2013, MNRAS, 435, 2903
Brown M. J. I. et al., 2008, ApJ, 682, 937
Cautun M., van de Weygaert R., Jones B. J. T., 2012, MNRAS, 429, 1286
Cautun M., van de Weygaert R., Jones B. J. T., Frenk C. S., 2014, MNRAS, 441, 2923
Chabrier G., 2003, PASP, 115, 763
Chen Y.-C. et al., 2015, preprint (arXiv:1509.06376)
Codis S., Pichon C., Pogosyan D., 2015, MNRAS, 452, 3369
Colberg J. M., 2007, MNRAS, 375, 337
Darvish B., Sobral D., Mobasher B., Scoville N. Z., Best P., Sales L. V., Smail I., 2014, ApJ, 796, 51
Davies L. J. M. et al., 2015, MNRAS, 452, 616
Dekel A., Birnboim Y., 2006, MNRAS, 368, 2
Dolag K., Meneghetti M., Moscardini L., Rasia E., Bonaldi A., 2006, MNRAS, 370, 656
Doroshkevich A., Tucker D. L., Allam S., Way M. J., 2004, A&A, 418, 7
Driver S. P. et al., 2009, Astron. Geophys., 50, 12
Driver S. P. et al., 2011, MNRAS, 413, 971
Driver S. P. et al., 2016, MNRAS, 455, 3911
Eardley E. et al., 2015, MNRAS, 448, 3665
El-Ad H., Piran T., 1997, ApJ, 491, 421
Ellison S. L., Patton D. R., Simard L., McConnachie A. W., 2008, AJ, 135, 1877
Fadda D., Biviano A., Marleau F. R., Storrie-Lombardi L. J., Durret F., 2008, ApJ, 672, L9
Forero-Romero J. E., Hoffman Y., Gottlöber S., Klypin A., Yepes G., 2009, MNRAS, 396, 1815
Gilbank D. G., Baldry I. K., Balogh M. L., Glazebrook K., Bower R. G., 2010, MNRAS, 405, no
Gray W. J., Scannapieco E., 2013, ApJ, 768, 174
Grootes M. W., Tuffs R. J., Popescu C. C., Robotham A. S. G., Seibert M., Kelvin L. S., 2014, MNRAS, 437, 3883
Gunawardhana M. L. P. et al., 2013, MNRAS, 433, 2764
Hahn O., Porciani C., Carollo C. M., Dekel A., 2007, MNRAS, 375, 489
Hopkins A. M. et al., 2013, MNRAS, 430, 2047
Kauffmann G. et al., 2003, MNRAS, 346, 1055
Kelvin L. S. et al., 2012, MNRAS, 421, 1007
Kennicutt R. C., Jr, 1998, ARA&A, 36, 189
Kereš D., Katz N., Weinberg D. H., Dave R., 2005, MNRAS, 363, 2
Kravtsov A. V., Borgani S., 2012, ARA&A, 50, 353
Kreckel K., Ryan Joung M., Cen R., 2011, ApJ, 735, 132
Kreckel K., Platen E., Aragón-Calvo M. A., van Gorkom J. H., van de Weygaert R., van der Hulst J. M., Beygu B., 2012, AJ, 144, 16
Lintott C. et al., 2011, MNRAS, 410, 166
Liske J. et al., 2015, MNRAS, 452, 2087
Mahajan S., Raychaudhury S., Pimbblet K. A., 2012, MNRAS, 427, 1252
Martin D. C. et al., 2005, ApJ, 619, L1
Morrissey P. et al., 2007, ApJS, 173, 682
Nelder J. A., Mead R., 1965, Comput. J., 7, 308
Nelson D., Vogelsberger M., Genel S., Sijacki D., Kereš D., Springel V., Hernquist L., 2013, MNRAS, 429, 3353
Neyrinck M. C., 2008, MNRAS, 386, 2101
Noeske K. G. et al., 2007, ApJ, 660, L43
Penny S. J. et al., 2015, MNRAS, 453, 3520
Pichon C., Pogosyan D., Kimm T., Slyz A., Devriendt J., Dubois Y., 2011, MNRAS, 418, 2493
Platen E., Van De Weygaert R., Jones B. J. T., 2007, MNRAS, 380, 551
Popescu C. C., Tuffs R. J., Dopita M. A., Fischera J., Kylafis N. D., Madore B. F., 2011, A&A, 527, A109
Porter S. C., Raychaudhury S., Pimbblet K. A., Drinkwater M. J., 2008, MNRAS, 388, 1152
Ricciardelli E., Cava A., Varela J., Quilis V., 2014, MNRAS, 445, 4045
Robotham A., Obreschkow D., 2015, PASA, 32, e033
Robotham A. S. G. et al., 2011, MNRAS, 416, 2640
Robotham A. S. G. et al., 2013, MNRAS, 431, 167
Rojas R. R., Vogeley M. S., Hoyle F., Brinkmann J., 2004, ApJ, 617, 50
Rojas R. R., Vogeley M. S., Hoyle F., Brinkmann J., 2005, ApJ, 624, 571
Salim S. et al., 2007, ApJS, 173, 267
Salpeter E. E., 1955, ApJ, 121, 161
Schlegel D. J., Finkbeiner D. P., Davis M., 1998, ApJ, 500, 525
Schwarz G., 1978, Ann. Statist., 6, 461
Shandarin S. F., Zeldovich Y. B., 1989, Rev. Mod. Phys., 61, 185
Snedden A., Coughlin J., Phillips L. A., Mathews G., Suh I.-S., 2016, MNRAS, 455, 2804
Sousbie T., 2011, MNRAS, 414, 350
Taylor E. N. et al., 2011, MNRAS, 418, 1587
Tempel E., Stoica R. S., Martinez V. J., Liivamagi L. J., Castellan G., Saar E., 2014, MNRAS, 438, 3465
Tuffs R. J., Popescu C. C., Vlk H. J., Kylafis N. D., Dopita M. A., 2004, A&A, 419, 821
Welker C., Dubois Y., Devriendt J., Pichon C., Kaviraj S., Peirani S., 2015, preprint (arXiv:1502.05053)
Whitaker K. E., van Dokkum P. G., Brammer G., Franx M., 2012, ApJ, 754, L29
Wijesinghe D. B. et al., 2012, MNRAS, 423, 3679
Wyder T. K. et al., 2007, ApJS, 173, 293
Yang X., Mo H. J., van den Bosch F. C., 2009, ApJ, 695, 900
Zehavi I. et al., 2011, ApJ, 736, 59
Zel'dovich Y., 1970, A&A, 5
Zheng Z., Zehavi I., Eisenstein D. J., Weinberg D. H., Jing Y. P., 2009, ApJ, 707, 554
Zinger E., Dekel A., Birnboim Y., Kravtsov A., Nagai D., 2015, preprint (arXiv:1510.05388)

This paper has been typeset from a TEX/LATEX file prepared by the author.